

Designing Quaternary Hydrides with Potential High T_c Superconductivity

Adam Denchfield,¹ Russell J. Hemley,^{1,2,3} and Hyowon Park^{1,4}

¹*Department of Physics, University of Illinois Chicago, Chicago, Illinois 60607, USA*

²*Department of Chemistry, University of Illinois Chicago, Chicago, Illinois 60607, USA*

³*Department of Earth and Environmental Sciences,
University of Illinois Chicago, Chicago, Illinois 60607, USA*

⁴*Materials Science Division, Argonne National Laboratory, Lemont, Illinois 60439, USA*

(Dated: July 1st, 2024)

While hydrogen-rich materials have been demonstrated to exhibit high T_c superconductivity at high pressures, there is an ongoing search for ternary and quaternary hydrides that achieve such high critical temperatures at much lower pressures. First-principles searches are impeded by the computational complexity of solving the Eliashberg equations for large, complex crystal structures. Here, we adopt a simplified approach using electronic indicators previously established to be correlated with superconductivity in hydrides. This is used to study complex hydride structures, which are predicted to exhibit promisingly high critical temperatures for superconductivity. In particular, we propose three classes of hydrides inspired by the FCC RH_3 structures that exhibit strong hydrogen network connectivity, as defined through the electron localization function. The first class $[\text{RH}_{11}\text{X}_3\text{Y}]$ is based on a $\text{Pm}\bar{3}\text{m}$ structure showing moderately high T_c , where the T_c estimate from electronic properties is compared with direct Eliashberg calculations and found to be surprisingly accurate. The second class of structures $[(\text{RH}_{11})_2\text{X}_6\text{YZ}]$ improves on this with promisingly high density of states with dominant hydrogen character at the Fermi energy, typically enhancing T_c . The third class $[(\text{R}^1\text{H}_{11})(\text{R}^2\text{H}_{11})\text{X}_6\text{YZ}]$ improves the strong hydrogen network connectivity by introducing anisotropy in the hydrogen network through a specific doping pattern. These model structures and the design principles provide the enough flexibility to optimize both T_c and the structural stability of complex hydrides.

The synthesis of materials that superconduct at room temperature and atmospheric pressure has been a long-standing dream since the discovery of superconductivity [1]. The theoretical predictions of high T_c superconductivity in metallic hydrogen [2, 3] and its subsequent prediction in dense hydrogen-rich materials [4] have been realized experimentally [5–9] (see [10] for a review), alongside theoretical work. Notable in this regard are predictions of extremely high- T_c superconductivity in LaH_{10} [11, 12] which were found to agree closely with experiment [5, 6], followed by later experiments on the YH_n system [7–9] and ternary hydrides [13–15]. Several more recent studies have proposed ternary or more complex hydrides as vehicles to lower the pressure needed for very high-temperature superconductivity [16–22].

Many such studies start with the highest T_c stoichiometric compounds and examine alloying effects that lower the pressure necessary to stabilize their structures. An alternative approach is to begin with hydrogen-rich MH_3 units that are already stable at ambient conditions and embed them in supercells designed to maximize T_c , as alluded to in Ref. [4] and explored in a recent computational study of $[\text{Al,Ga}]\text{H}_3$ alloys [22]. The FCC rare-earth trihydride (RH_3 ; $\text{R}=\text{Sc,Y,La-Lu}$) compounds have strong electron-phonon coupling (EPC) [23–27] associated primarily with octahedrally coordinated hydrogen, as in palladium hydrides [28]. Notably, experiments on YH_3 indicate that the FCC phase can be metastabilized with doping [29, 30], ball milling [31], and quenching [32]. In FCC RH_3 , doping the rare earth [33] and substituting nitrogen for octahedral hydrogen in LuH_3 [34, 35] have both been predicted to increase

this electron-phonon coupling. Notably, evidence of superconductivity in near-ambient conditions has been reported for FCC $\text{LuH}_{3-x}\text{N}_y$ [36, 37] with 0.8% N by weight. Other experiments indicate that the FCC phase of N-doped $\text{LuH}_{3-\delta}$ can be recovered to ambient conditions [38] and displays nearly-flat electronic bands just under the Fermi energy E_F [39]. Nearly-flat bands were first predicted in $\text{Fm}\bar{3}\text{m}$ $\text{Lu}_8\text{H}_{23}\text{N}$ [40] which is predicted to be dynamically stable at 2 GPa when including nuclear quantum effects [41].

Inspired by the above work, we generalize the idea of doping the metal atom in RH_3 to include small amounts of doping of the octahedral hydrogen with Lewis bases [O,N,S,P]. As the space of possible quaternary structures and stoichiometries is huge, we use FCC RH_3 and the structural motif from our previous work [40] to design model structures with relatively few degrees of freedom. Specifically, we propose three model structures of increasing complexity that are engineered to have dominant hydrogen states at the E_F that emulate metallic hydrogen [4]. These structures are summarized in Fig. 1. When discussing specific examples, we use these structures as starting points and perform DFT variable-cell relaxations. We estimate T_c using a linear correlation observed between Eliashberg T_c and a quantity Φ based on electronic properties of the hydrogen sublattice in hydrides (see *Materials and Methods*). We also perform frozen phonon calculations near ambient pressures to examine the dynamical stability of selected structures.

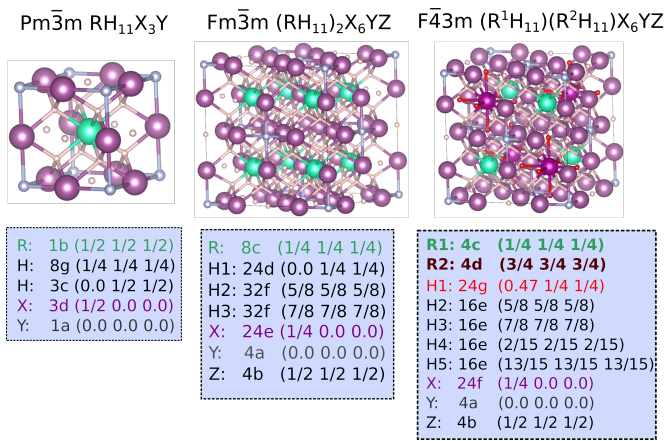


FIG. 1: Three structures of increasing complexity that serve as model structures for quaternary (or even more complex) hydrides.

RESULTS

Pm $\bar{3}m$ RH₁₁X₃Y Structure

We present first a simple model structure for quaternary hydrides, with the chemical formula RH₁₁X₃Y (Fig. 2). It is distinguished by a central RH₁₁ unit with a typical electron localization function (ELF) and projected density of states (PDOS) illustrated using LuH₁₁ as an example in Fig. 2(c,d) surrounded by an X₃Y 'cage'. In the RH₁₁X₃Y model structure, the hydrogens are placed in the positions they occupy in FCC RH₃, except for the 1a Wyckoff position which may be occupied by hydrogen or a Lewis base (N,P,O,S). The 3d Wyckoff positions are also kept unspecified, but the intent for these atoms is to stabilize the FCC lattice. Choices of X and Y are also intended to make the X₃Y cage inert such the chemical bonding of the central RH₁₁ unit (and therefore its superconducting properties) is preserved. We explore the effects of filling the X and Y positions and hole doping in Fig. S5 (see SI), finding that the addition of trivalent X atoms typically leads to strong H bonding, bringing the hydrogen states far below E_F. Hole-doping and filling Y=O both result in hydrogen states dominating the DOS(E_F), though not at the same magnitude as LuH₁₁ [Fig. 2(d)]. These structures are simple enough to perform Eliashberg calculations for T_c, unlike the more complex structures discussed later. For the latter, estimate the critical temperature for hydride superconductors based on electronic indicators [42], which we refer to as T_c^{net}.

We first note that the networking-value T_c^{net} [(6)] was found to be within ± 60 K of isotropic Eliashberg T_c^{Eli} calculations for 300 hydrides [42]. Calculations since then have verified its accuracy at predicting Eliashberg T_cs for CaH₆ (T_c^{Eli}: 236 K, T_c^{net}: 264 K) [43] and Lu₄H₁₁N (T_c^{Eli}: 100 K, T_c^{net}: 99 K) [44]. As a check on the T_c estimation process, we estimate (6) for Fm $\bar{3}m$ LuH₁₀ (see

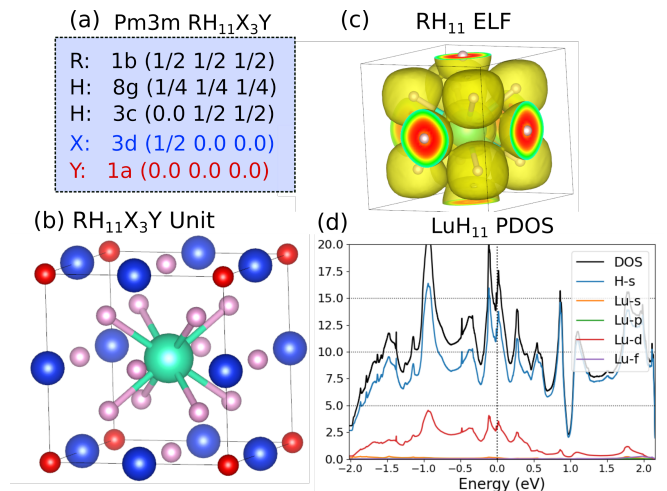


FIG. 2: Proposed RH₁₁X₃Y structure. (a) Structural parameters, (b) Visualization of the RH₁₁X₃Y unit cell, (c) Example electron-localization-function (ELF) of LuH₁₁ at an isovalue of 0.55, (d) PDOS of the example LuH₁₁ showing metallic hydrogen states dominant at E_F.

Fig. S4) at 150 GPa ($a = 4.91$ Å) gives T_c^{net} \approx 339 K compared to the Eliashberg T_c^{Eli} = 289 K ($\lambda \approx 3.5$) for Fm $\bar{3}m$ LuH₁₀ at 175 GPa [44]. Additionally, our LuH₁₁ unit in Fig. 2 ($a = 5.21$ Å) is estimated to have a T_c^{net} of 266 K. Our hypothesis is that any structure with similar chemical tendencies as these FCC RH₁₁ units would have a T_c in a similar range. We note the similarity to the T_c range reported experimentally for Lu-H-N [37].

Lu₄H₁₁O Example

As a reference for structural, electronic and Eliashberg calculations, we choose the example Pm $\bar{3}m$ Lu₄H₁₁O (Fig. 3). The calculated DOS of the structure near E_F is dominated by hydrogen states [DOS_H(E_F) \sim 0.5], meaning its predicted T_c should be higher than that of Lu₄H₁₁N [44] [DOS_H(E_F) \sim 0.33]. This arises from the difference in ionic bonding strength of O compared to N. We find through the ELF that the $\phi_{net}^{crit} = 0.521$, with the networking value predicted T_c^{net} = 130 K. Pm $\bar{3}m$ Lu₄H₁₁O features a nearly-flat electron band 0.36 eV below E_F (around X) [Fig. 3(c)] which is expected to contribute to the superconductivity due to the high energy of phonons around 12-15 THz (about 0.08 eV) and 35 THz (0.15 eV). We find increasing correlation effects via DFT+U (U_d = 5.5 on Lu) can induce Lifshitz transitions [Fig. 3(c)] indicating correlation effects could increase the EPC. Density functional perturbation theory calculations on a 4x4x4 q-point mesh indicate it is dynamically stable above 25 GPa. We used the EPW code [45] to interpolate the electron-phonon matrix elements using Wannier functions, with k/q meshes of 32³ and 16³. The $\alpha^2F(\omega)$ leads to a large integrated electron-phonon

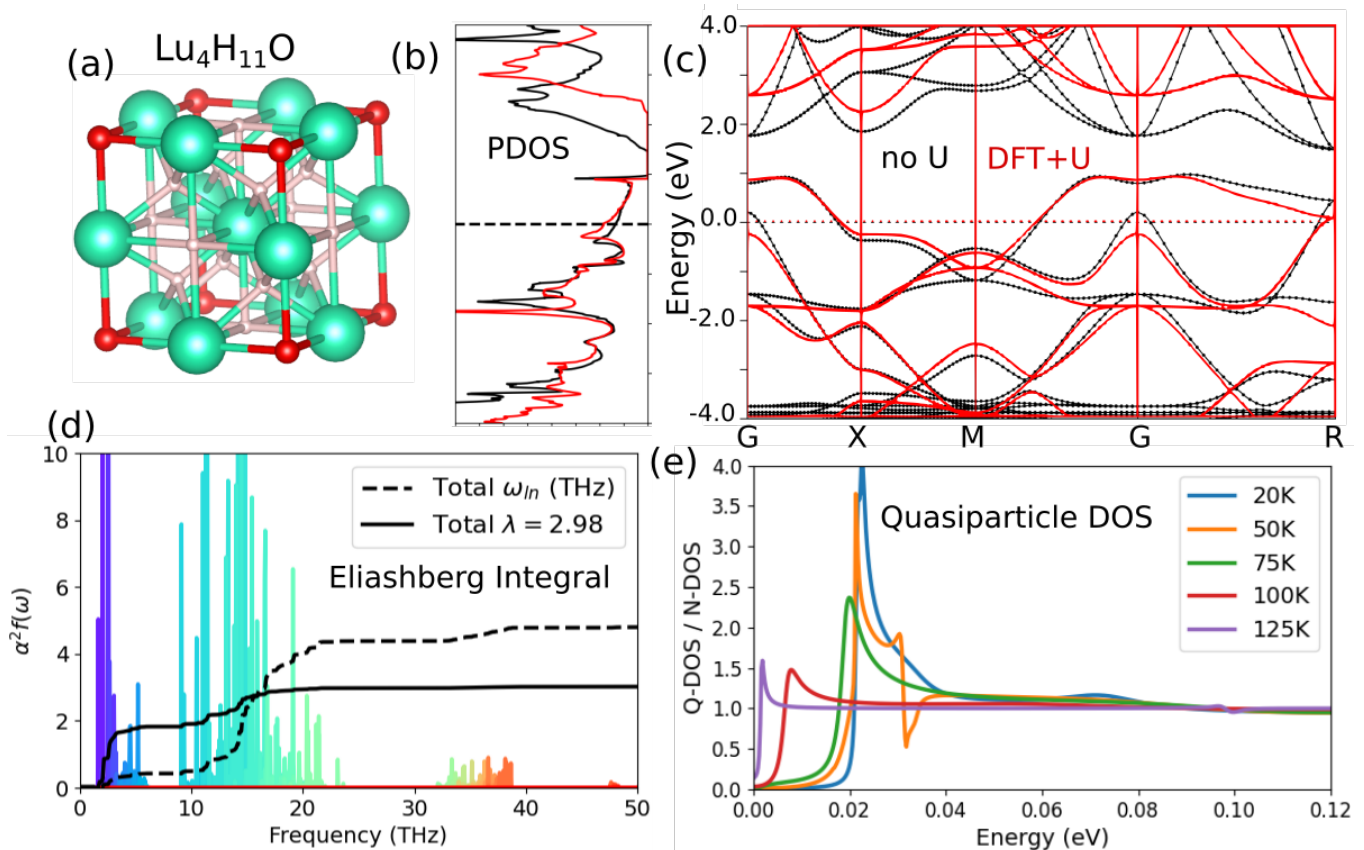


FIG. 3: Electronic, structural, and superconducting properties of Pm3m Lu₄H₁₁O. (a) Visualization of the unit cell. (b) PDOS at 17 GPa with and without +U. (c) Band structures with and without +U. (d) $\alpha^2 F(\omega)$, integrated $\lambda(\omega)$, and integrated $\omega_{ln}(\omega)$ after convergence studies. (e) Quasiparticle density of states (QDOS) relative to the normal-state DOS.

coupling of $\lambda \approx 3$ [Fig. 3(d)] and $\omega_{log} \approx 5$ THz, with an Allen-Dynes T_c (see Eq. 1) of 90 K using $\mu = 0.10$ [46]. The Allen-Dynes T_c decreases to 50 K if not converged (e.g. using a coarser mesh and larger thermal broadening factor). The T_c has sizable contributions from the octahedral hydrogen modes below 5 THz and 12-15 THz, with a small contribution to ω_{log} from higher-frequency tetrahedral hydrogen modes at 35 THz.

We performed anisotropic Eliashberg calculations as implemented in the EPW software [47] and compute the quasiparticle DOS in the superconducting state at various temperatures, illustrating the gap closure around 125 K [Fig. 3(g)] which coincides with the T_c^{net} of 130 K predicted by (6). The sizable difference between the Allen-Dynes and Eliashberg T_c may reflect that the Allen-Dynes formula was created from fitting to alloys of conventional superconductors [46] with lower phonon frequencies, and so the high frequency modes here (15 THz and 35 THz) may not be appropriately captured in these fits. The phonon dispersion, superconducting properties, and effect of doping are further elucidated in the Supplementary Information.

Other $RH_{11}X_3Y$ Examples

Both LuH₁₁Ca₃O and CaH₁₁Y₃O have dominant $DOS_H(E_F)$ and end up having similar T_c^{net} despite the almost threefold difference in their total $DOS_{tot}(E_F)$ (Fig. S6, SI). We emphasize this is due to the observation that T_c is not correlated with the total $DOS(E_F)$ in hydrides, but the relative hydrogen contribution [42]. We also

As boron is known to attain an oxidation state as low as B⁵⁻, we also explored Lu₄H₁₁B (Fig. S7, SI) and found an interesting flat band near E_F of Lu-d, H-s, and B-p character which remained under relaxation that would likely lead to an instability of some kind. We also found SiH₁₁Lu₃N to have a hybridized nearly-flat band near E_F (Fig. S22, SI) with $T_c^{net} = 90$ K. As their predicted T_c^{net} are below 200 K we did not further examine these examples. We confirm there is no DFT+U dependence for these results (the Fermi level properties do not change).

Selected examples discussed so far as well as the others we explore later are outlined in Table I, with some relative energies of formation computed in Table S1. The results establish that while the first model structure (Fig.

TABLE I: Table of selected materials, with the parent structure, computed electronic properties, and estimated^a T_c

Parent Structure	Material	a (Å)	$DOS_H(E_F)$	ϕ_{net}^{crit}	T_c^{net} (K)	Notes
RH ₁₁ X ₃ Y	Lu ₄ H ₁₁ O	5.01	0.66	0.50	130	$T_c^{Eli} = 125$ K with frequency-dependent s-wave gap
	LuH ₁₁ Ca ₃ O	5.11	0.62	0.52	145	
	CaH ₁₁ Y ₃ O	5.14	0.66	0.485	130	
	ScH ₁₁ Y ₃ N	5.05	0.5	0.495	120	
	SiH ₁₁ Lu ₃ N	4.90	0.4	0.47	90	T_c^{net} rises to 125 K with a supercell distortion
(RH ₁₁) ₂ X ₆ YZ	Lu ₈ H ₂₃ N	10.04	0.74	0.515	165-180	Dynamically stable at 2 GPa due to quantum effects
	Lu ₈ H ₂₂ N	10.07	0.7	0.52	160	$T_c^{net} = 215$ K with classical distortion and doping
	Sc ₆ Ca ₂ H ₂₃ N	9.60	0.5	0.582	160	$T_c^{net} = 220$ K with classical distortion
	Y ₆ Mg ₂ H ₂₃ O	10.07	0.8	0.50	165-170	$T_c^{net} = 170$ K by removing 4b-H
	Y ₆ Ca ₂ H ₂₂ N ($U_{Y_d} = 3.5$ eV)	10.32	0.85	0.51	165	Removed 4b-H
	Mg ₆ La ₂ H ₂₃ O	10.05	0.77	0.575	200	Most likely unstable
	Mg ₆ Sc ₂ H ₂₃ O	9.50	0.77	0.575	200	Most likely unstable
(R ¹ H ₁₁)(R ² H ₁₁)X ₆ YZ	Y ₇ LiH ₂₃ N	10.18	0.66	0.55	170	Hydrogen sublattice may distort, remains metallic
	Y ₇ LiH ₂₃ N ($U_{Y_d} = 3.5$ eV)	10.18	0.79	0.54	185-220	$T_c^{net} = 220$ K with electron doping
	Y ₇ LiH ₂₂ N (removed 4b-H)	10.22	0.66	0.61	190-220	$T_c^{net} = 220$ K with electron doping
	Y ₇ CaH ₂₃ N	10.24	0.65	0.56	180-200	$T_c^{net} = 200$ K with electron doping
	Lu ₇ SiH ₂₃ N	9.96	0.5	0.55	150	
	Sc ₇ LiH ₂₃ N	9.33	0.48	0.655	190	ScH ₃ -based compounds may need 20-40 GPa
	Sc ₇ LiH ₂₃ N ($U_{Sc_d} = 5$ eV)	9.33	0.51	0.65	195	
	Sc ₇ NaH ₂₃ N	9.43	0.51	0.63	185	
	Sc ₇ NaH ₂₃ N ($U_{Sc_d} = 5$ eV)	9.43	0.64	0.62	205	
	Sc ₇ MgH ₂₃ N ($U_{Sc_d} = 5$ eV)	9.43	0.7	0.64	220-230	$T_c^{net} = 230$ with electron doping

^a The estimated T_c^{net} is rounded to the nearest 5 K with an error bound of ± 60 K [42].

2) can result in hydrogen-dominant states at E_F , the magnitude of the $DOS(E_F)$ is not comparable to that of the core RH₁₁ structure; the $DOS_{H,rel}(E_F)$ ratio is not typically close to 1, which limits the achievable T_c^{net} (Eq. 6).

Fm $\bar{3}m$ (RH₁₁)₂X₆YZ Structure

Using T_c^{net} [(6)] as a guiding principle, we build on the simple RH₁₁X₃Y structure (Fig. 2) and design a supercell to increase H_f and $DOS_H(E_F)$. The increased H_f requires less [O,N,S,P], and we hypothesize that high symmetry Fm $\bar{3}m$ structures inspired by our previous work [40, 41] will lead to large $DOS_H(E_F)$ by bringing tetrahedral hydrogen states to E_F . This leads to a supercell in which charge is redirected away from the X₃Y cage surrounding the RH₁₁ unit [Fig. 4(a-b)]. We visualize and specify a model structure meeting these requirements in Fig. 4(c,d). The blue regions indicate the RH₁₁ regions.

Our second model structure (Fig. 4) is designed to emulate the hydrogen-dominated band structure near E_F of the core RH₁₁ units, with the appropriate choice of X,Y, and Z atoms. The chemical formula is (RH₁₁)₂X₆YZ, where R is an atom in the 8c position, X is an atom stabilizing the FCC RH₁₁ lattice in the 24e position with $x \approx 0.25$, and Y,Z in the 4a/4b positions ensure the X atoms are inert with respect to the RH₁₁ lattice. The hydrogens occupy two 32f positions with $x \approx 0.875$ and $x \approx 0.625$ as well as the 24d positions. Figure S12 shows four examples without relaxing the structure from the parameters given in Fig. 4(d). Their electronic proper-

ties suggest a high estimated T_c in the 150-170 K range using (6). However, these examples are unrelaxed so we do not quantify their properties further.

(CaH₁₁)₂ Sc₆NH Example

We start with an in-depth look at a particular example of the (RH₁₁)₂X₆YZ model structure. Choosing R=Ca, X=Sc, Y=N, and Z=H, we have (CaH₁₁)₂Sc₆NH, or Sc_{0.75}Ca_{0.25}H_{2.875}N_{0.125}. We focus on this example for a variety of reasons. In terms of stability, 25-33% Ca doping is predicted to decrease the pressure needed to stabilize cubic ScH₃ by over 10 GPa [33]. With respect to its potential for high- T_c superconductivity, CaH₆ has been shown to exhibit a T_c of 215 K [48] close to the original prediction [49] and possibly higher T_c with more hydrogen-rich compounds [50]. Additionally, doping CaH₆ with rare earths could achieve even higher T_c [51, 52]. Finally, these ingredients the following criteria: ScN is semiconducting, the Sc atoms will help stabilize the tetrahedral hydrogen in the CaH₁₁ unit, and the large electronegativity of N is expected to weaken the ionic bonding of Sc atoms with tetrahedral hydrogen, bringing tetrahedral hydrogen states higher in energy to hybridize with the octahedral hydrogen.

The electronic and phonon properties of (CaH₁₁)₂Sc₆NH at 20 GPa are shown in Fig. 5. The PDOS/bandstructure shows multiple hydrogen-dominant van Hove singularities (vHs) near E_F , reminiscent of the flat bands in Lu₈H₂₃N [40, 41]. We find $\phi_{net}^{crit} = 0.585$ and $T_c^{net} = 165$ K. Removing the 4b-H

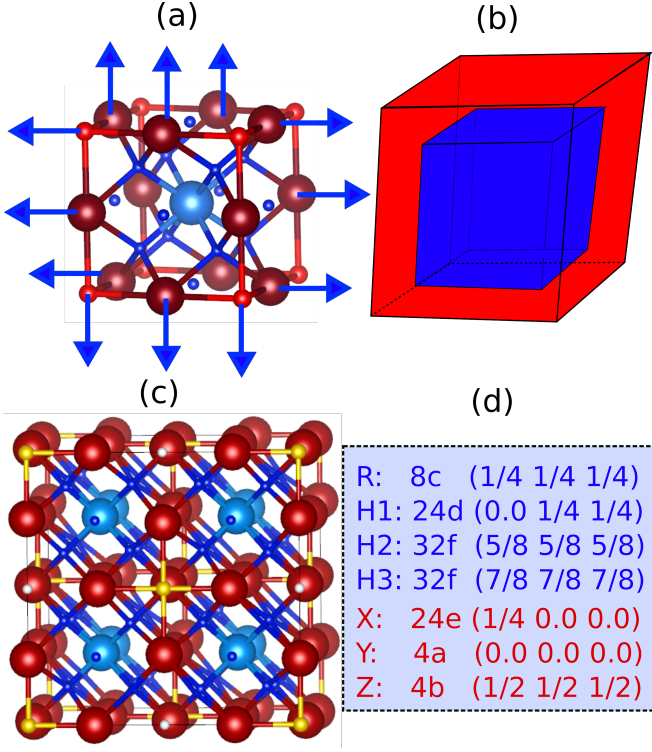


FIG. 4: Strategy for creating the $(RH_{11})_2X_6YZ$ structure. In this scheme we redirect the charge of X_3Y layers of the simple model structure (Fig. 2) away from the RH_{11} units. (a) Visualization of extra charge brought by 3d-X atoms being redirected away from the RH_{11} unit. (b) A depiction of an inert X_6YZ shell containing the RH_{11} unit. (c) Plot of $(RH_{11})_2X_6YZ$ using a similar coloring scheme as (b) to further illustrate the concept. (d) The Wyckoff positions of the quaternary structure. The atoms in (c) are colored as: 24e-X (red), 4a-Y (yellow), 4b-Z (white), and RH_{11} units (blue).

or replacing the nitrogen with oxygen both result in T_c^{net} rising to 180 K (Fig. S15). The imaginary phonon frequencies at Γ indicate there may be a structural instability of the hydrogen sublattice.

To evaluate the likelihood of quantum effects stabilizing this structure against such an instability, we evaluate the anharmonicity of the potential energy surface (PES) associated with displacing the crystal along the corresponding dynamical matrix eigenvector (visualized in the inset). We define the number of hydrogen strongly displaced in the mode to be all hydrogen whose displaced distance is more than $D_{max}/6$, where D_{max} is the maximum distance a hydrogen is displaced. We see the maximum energy gain at 20 (30) GPa is 7 (2) meV/hydrogen at an average hydrogen displacement of 0.22 (0.15) Å. The double well PES becomes more harmonic with increased pressure, but the wells deepen as pressure is decreased, similar to $Lu_8H_{23}N$ [41]. Fig. S13 shows examples of ground state densities computed for anhar-

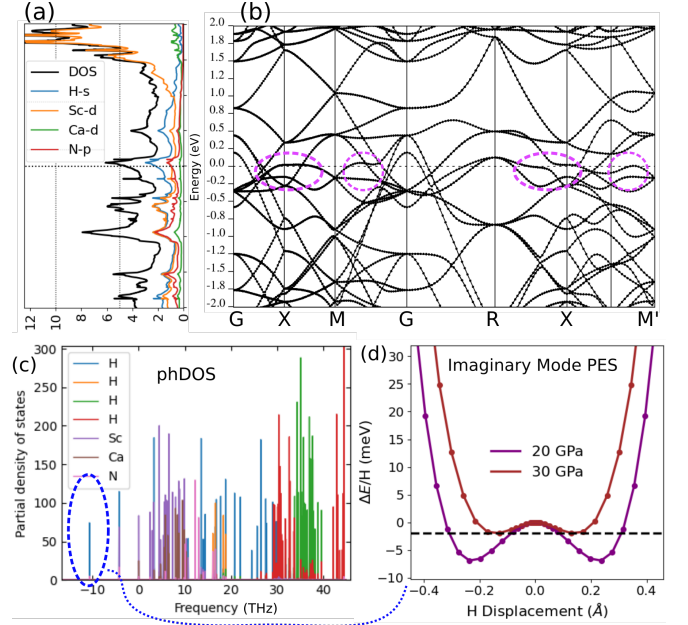


FIG. 5: Electronic density of states (a) and band structure (b) of $Sc_6Ca_2H_{23}N$ at 20 GPa, with several van Hove singularities near E_F circled, (c) Phonon density of states resolved by atomic projections of unique Wyckoff positions, (d) Potential energy surface (PES) of the mode with largest imaginary frequency at 20 and 30 GPa.

monic potentials; potentials can be surprisingly anharmonic while still favoring a centered wavefunction. These results indicate that nuclear quantum effects stabilize the structure against this instability at this or a slightly higher pressure. For pressure ranges where this distortion occurs, we find this distortion in fact could enhance T_c^{net} up to 220 K based on our calculations at 20 GPa (Fig. S2). For more information on this and related stoichiometries, see the Supplemental Information.

Other $(RH_{11})_2X_6YZ$ Examples

The electronic properties of twelve more examples are shown in Fig. S9. All twelve examples have hydrogen states dominant at E_F , which correlates with high T_c hydride superconductivity [42]. As H_f in (8) is nearly constant in these examples, the only remaining parameter to maximize T_c is ϕ_{iso}^{net} . Using this metric, we find the highest ϕ_{iso}^{net} values in the $(RH_{11})_2(Mg_6OH)$ systems, with a corresponding networking-value T_c^{net} of 200 K. For $R=La$ the high ϕ_{iso}^{net} responsible for this is attributed to hydrogens tetrahedrally oriented with respect to Mg bending away from the oxygen atoms and forming a body-centered cubic hydrogen cage (Fig. S20), with H-H distance 1.964Å between cube edges and 1.692Å between the vertices and the central H atom. Such small H-H distances have also been observed in some intermetal-

lic hydrides [53]. For $R=\text{Sc}$, the hydrogen cubic cage does not form, but the smaller lattice constant appears to make up for it in terms of high ϕ_{iso}^{net} values. Unfortunately, a stability analysis (see SI Section ‘‘Stability’’) indicates $([\text{La},\text{Sc}]\text{H}_{11})_2\text{Mg}_6\text{OH}$ are dynamically unstable. However, we note the ternary system $(\text{LuH}_{11})_2\text{Lu}_6\text{HN}$ was predicted to be dynamically stable at 2 GPa when considering quantum effects [41]. Clearly, fine-tuning of the stoichiometry can be a determining factor in each structure’s dynamical stability.

We find that structures with dominant hydrogen states at E_F can be obtained by choosing $X=\text{Sc}/\text{Y}/\text{La}/\text{Lu}$, $R=\text{Li}/\text{Na}/\text{Mg}/\text{Ca}/\text{Sr}/\text{Al}/\text{Ga}/\text{In}$, $Y=\text{H}/\text{O}/\text{S}/\text{N}/\text{P}$, and $Z=\text{H}$ or vacant (see SI). Swapping the role of the R and X atoms also results in hydrogen-dominant states at E_F (see SI), though dynamical and thermodynamic stability is in question.

The properties of a few $(\text{RH}_{11})_2\text{X}_6\text{YZ}$ examples are summarized in Table I. While T_c^{net} is generally higher for these examples the $\text{RH}_{11}\text{X}_3\text{Y}$ model structure, we find in $(\text{CaH}_{11})_2\text{Sc}_6\text{NH}$ that relaxation along instability pathways can in fact raise T_c^{net} through large increases in ϕ_{iso}^{net} (Fig. S2). A similar vibrational analysis on $(\text{LuH}_{11})_2\text{Lu}_6\text{N}$ also reveals a classical distortion [41], which coupled with fine-tuning of the doping level, raises T_c^{net} to 215 K. Based on these observations, we propose our last model structure, designed to increase ϕ_{iso}^{net} and therefore T_c^{net} .

$\text{F}\bar{4}3\text{m} (\text{R}^1\text{H}_{11})(\text{R}^2\text{H}_{11})\text{X}_6\text{YZ}$ Structure

This structure involves symmetry breaking of the 8c-R atoms of the previous model structure, captured with the formula $(\text{R}^1\text{H}_{11})(\text{R}^2\text{H}_{11})(\text{X}_6\text{YZ})$, where X is a rare earth atom, and R^1, R^2 are other electron-donating metal atoms (possibly the same as X). The Wyckoff positions are summarized in Fig. 1. The change in metal ion size enhances symmetry breaking of the 24d-H positions in the structure. Those hydrogen atoms are observed to shift to either R^1 or R^2 (typically whichever has more valence electrons). Fig. 1 shows the symmetry breaking hydrogens (red) as closer towards the 4d- R^2 atoms.

We use this generalization of the $\text{Fm}\bar{3}\text{m} (\text{RH}_{11})_2\text{X}_6\text{YZ}$ to simulate 12.5% doping of ternary $\text{R}_8\text{H}_{23}\text{N}$ structures, which involves choosing $X=\text{R}^2=\text{a rare earth}$, and R^1 a dopant atom.

Doping $\text{R}_8\text{H}_{23}\text{N}$

We begin with the interesting electronic structure of $\text{Lu}_8\text{H}_{23}\text{N}$ (A) [40] and investigate replacing Lu with Sc, Y. Cell relaxation was performed and the resulting PDOS and electronic properties are compared in Fig. S19 (see SI). U-values were chosen by performing DFT+U calculations on the rare earth nitrides and adjusting U_d to match the indirect band gaps to experiment [54]. For $\text{Y}_8\text{H}_{23}\text{N}$,

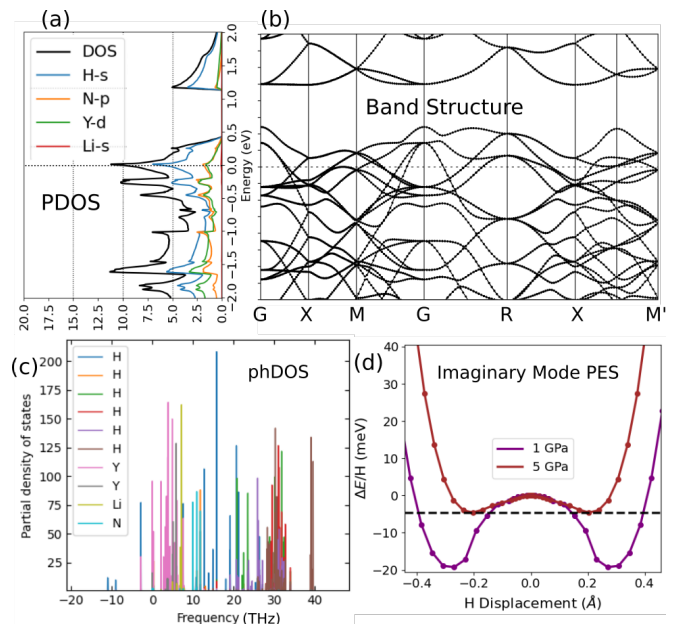


FIG. 6: Properties of $(\text{YLiH}_{22})(\text{Y}_6\text{NH})$ ($a = 10.1 \text{ \AA}$) (a) Electronic band structure and projected density of states, (b) Phonon density of states resolved by atomic projections of unique Wyckoff positions, (c) Potential energy surface (PES) of the mode with largest imaginary frequency at 1 GPa and 5 GPa.

while the flat hydrogen band is still present near E_F , the larger lattice constant results in a smaller ϕ_{iso}^{net} , lowering the estimated T_c^{net} . For $\text{Sc}_8\text{H}_{23}\text{N}$ the much smaller lattice constant leads to a higher ϕ_{iso}^{net} but the Sc_d orbitals hybridizing with the Fermi level leads to more charge screening of the negative nitrogen atoms. This brings hydrogen states below E_F and weakens the flatness of the hydrogen band.

Given that doping YH_3 assists in stabilizing the FCC phase [29, 55–57] and various studies indicate doping rare-earth hydrides yields high T_c s [33, 58, 59], we investigate the effects of substituting some $R=[\text{Sc},\text{Y}]$ atoms in $\text{R}_8\text{H}_{23}\text{N}$ with alkali and alkali earth atoms. In particular, we investigate Li, Na, and Mg doping in $\text{Sc}_8\text{H}_{23}\text{N}$, and Li, Mg, and Ca doping in $\text{Y}_8\text{H}_{23}\text{N}$. We start with the parent structure in Fig. 1(right) using $X=\text{Sc}/\text{Y}, \text{R}^1=\text{D}$ (dopant), $\text{R}^2=\text{Sc}/\text{Y}, \text{Y}=\text{H}, \text{Z}=\text{N}$, with the R^1 position occupied by either a dopant $\text{D}=\text{Li}/\text{Mg}/\text{Ca}$ or Sc/Y for lower dopant concentrations.

$(\text{YH}_{11})(\text{LiH}_{11})\text{Y}_6\text{HN}$ Example

A representative example of the $\text{F}\bar{4}3\text{m}$ model structure [Fig. 1(right)] is $(\text{YH}_{11})(\text{LiH}_{11})\text{Y}_6\text{HN}$ (or $\text{Y}_{0.875}\text{Li}_{0.125}\text{H}_{2.875}\text{N}_{0.125}$), which has a lattice constant of 10.1 Å whose stoichiometry is similar to an experimentally stable cubic structure $\text{Y}_{0.9}\text{Li}_{0.1}\text{H}_{2.8}$ [30]. Figure 6 illustrates its electronic and vibrational properties via

DFT and frozen phonon calculations [60]. As in previous examples, the $\text{DOS}_H(E_F)$ is high and dominant [Fig. 6(a)], with contributions from all hydrogen, though the largest contribution is from the 4b-H. The band structure illustrates a propensity of vHs near E_F , as well as flat band regions 0.3 eV below and 1.1 eV above E_F [Fig. 6(b)]. As designed, the symmetry-broken octahedral hydrogen improve the connectivity of the hydrogen sublattice, increasing ϕ_{iso}^{net} to 0.6 (note our record of ϕ_{iso}^{net} for Y-based hydrides using the previous structure was 0.55; see Fig. S9). This increases T_c^{net} to 185 K, which may be increased by pressure and further fine-tuning of the stoichiometry. We find electron doping can increase T_c^{net} up to 220 K.

Since the zero pressure phonon calculation reveals imaginary modes [Fig. 6(c)], we perform an anharmonicity analysis as was done previously for $(\text{CaH}_{11})_2\text{Sc}_6\text{NH}$ (Fig. 5). Here we find another double well, which at 1 GPa is quite deep but becomes nearly flat at 5 GPa [Fig. 6(d)]. All frequencies are positive at 15 GPa, implying the high-symmetry $F\bar{4}3m$ structure becomes dynamically stable in the 5-15 GPa range. The distortion expected to occur below 5 GPa features octahedral hydrogen bending towards tetrahedral hydrogen, which is expected to anisotropically change ϕ_{iso}^{net} . We find the distortion at 1 GPa to have a fairly negligible effect on the PDOS like in $(\text{CaH}_{11})_2\text{Sc}_6\text{NH}$, but the T_c^{net} drops to 145 K due to an undesirable anisotropy in ϕ_{net}^{crit} .

Various perturbations on $(\text{YH}_{11})(\text{LiH}_{11})\text{Y}_6\text{HN}$ also seem to yield high T_c^{net} . Removing the 4b-H yields $F\bar{4}3m$ $\text{Y}_{0.875}\text{Li}_{0.125}\text{H}_{2.75}\text{N}_{0.125}$ with $T_c^{net} = 200$ K and a similar double well PES for the mode with largest imaginary frequency (Fig. S3). The primary difference from removing the 4b-H is the DOS is fairly flat around E_F , but an extremely flat hydrogen-based band exists 1 eV above E_F , corresponding to ‘hydrogen-cage-like’ nearly-localized electronic states. Further changing one of the 4a-N to a hydrogen atom effectively electron-dopes the system, which also has a high T_c^{net} of 200 K after relaxation.

Other $(R^1\text{H}_{11})(R^2\text{H}_{11})\text{X}_6\text{YZ}$ Examples

$(\text{YH}_{11})(\text{CaH}_{11})\text{Y}_6\text{HN}$ has a comparatively modest ϕ_{iso}^{net} of 0.56 and T_c^{net} of 180 K [Fig. S16]. We proceed with Sc-based examples, as the reduced lattice constant generally favors high ϕ_{iso}^{net} . Our remaining examples involve doping $\text{Sc}_8\text{H}_{23}\text{N}$ to form $F\bar{4}3m$ $\text{Sc}_7[\text{Li,Na,Mg}]\text{H}_{23}\text{N}$. The electronic and lattice parameters, and T_c estimates are shown in Table I with PDOS plots in the SI. Behavior similar to Li-doped $\text{Y}_8\text{H}_{23}\text{N}$ occurs with H shifting towards the 4d-Sc Wyckoff positions. This change coupled with the smaller lattice constant of the FCC ScH_3 parent structure leads to large ϕ_{iso}^{net} due to the robust hydrogen network that forms around the 4d-Sc positions.

We summarize the properties of these examples in Table I. The T_c estimates of 185-230 K for these structures

illustrate the power of combining both nitrogen and alkali metal dopants in this structure design, enabling heightened ϕ_{iso}^{net} . We mention we briefly investigated replacing N with S, and found $F\bar{4}3m$ $\text{Sc}_7\text{MgH}_{23}\text{S}$ is insulating but with a high $\phi_{iso}^{net} = 0.655$. Hole-doping, for example with further Mg (perhaps using $\text{Fm}\bar{3}m$ $(\text{MgH}_{11})_2\text{Sc}_6\text{SH}$) would create a metal with hydrogen-dominant states.

Discussion

In the search for hydride superconductors with very high T_c , a complicating factor is the necessity to include quantum zero-point motion/energy and thermal effects. Without such effects, harmonic phonons with classical nuclei often overestimate structural instabilities for high T_c hydrides [61, 62]. In fact, T_c tends to be highest when the system is closest to structural transitions [63] (and where DFT methods can fail). Another complicating factor for first principles searches is that of metastability; it may prove sufficient for experimental purposes to produce a metastable superconductor (so long as its lifetime is measured in months or years), yet such structures would be discarded in many computational structure searches. We therefore take a different approach and design complex hydride structures with the intent of producing electronic properties that correlate with high T_c [42]. We use FCC RH_3 as the parent structure, as these structures have high EPC and can be stabilized at ambient pressures in a variety of ways [31–33, 38, 55].

We have proposed three successively more chemically complex model hydride structures with predicted T_c^{net} maximized by having hydrogen-dominant states at E_F and a strongly connected hydrogen sublattice. The three models exhibit increased flexibility for tuning stability and T_c relative to simple binary structures. Examples within each model structure are candidate high T_c superconductors that are potentially stable near ambient pressure and therefore deserve additional study.

Compounds based on the first and simplest model structure show moderate promise in producing ternary/quaternary hydride superconductors with T_c in the 100-150 K range and are potentially metastable near ambient pressures. We find $\text{Pm}\bar{3}m$ $\text{Lu}_4\text{H}_{11}\text{O}$ has a lower formation energy than $\text{LuH}_3 + 3\text{LuH}_2 + \text{H}_2\text{O}$ by 0.128 eV/atom (Table S1). We also note YH_3 and Y_2O_3 are known to react to form cubic YH_xO_y under heating [64]. The second and third model structures of quaternary hydrides have enough flexibility to optimize parameters going into the T_c^{net} estimator, which we use to generate examples with upper estimated T_c^{net} s up to 220-230 K at near-ambient pressures when accounting for hydrogen distortions. While the examples discussed are not on the convex hull (Table S1), this does not discount their possible metastability. For example, diamond is also 0.14 eV/atom above its convex hull using data from Ref. [65].

The second model can produce compounds with high

T_c^{net} stable at low pressures, as $\text{Lu}_8\text{H}_{23}\text{N}$ (A) studied by us previously [40] was shown to be dynamically stable at 2 GPa when nuclear quantum effects are included [41]. Recently, N-doped FCC LuH_3 has been observed to be recoverable to ambient [38] using the techniques in Ref. [32]. Our $\text{Fm}\bar{3}\text{m}$ $(\text{CaH}_{11})_2\text{Sc}_6\text{NH}$ example is expected to be dynamically stable above 20 GPa when nuclear quantum effects are included. As the double well is deepened (from i.e. lower pressure) the octahedral hydrogen are expected to distort from high symmetry positions which surprisingly increases T_c^{net} , with a pressure regime where spectroscopic signatures are broadened due to quantum ZPM. This interpretation on the structural dynamics is supported by high-pressure studies of ScH_3 [66].

Our third model structure involves complexity higher than quaternary systems. Nevertheless, we limit ourselves to the quaternary case by analyzing the doping of $[\text{Sc}/\text{Y}]_8\text{H}_{23}\text{N}$ structures. The structure is designed to distort hydrogen to increase ϕ_{iso}^{net} with many possible dopants. Based on our calculations on cubic $\text{Y}_{0.875}\text{Li}_{0.125}\text{H}_{2.875-\delta}\text{N}_{0.125-\epsilon}$ structures, we predict T_c to have a maximum of $220\text{ K} \pm 60\text{ K}$ at a pressure between 5-15 GPa for optimal δ, ϵ . For synthesis we recommend leveraging the approaches used in Refs. [30, 32, 38]. At lower pressures, distortions away from the $\text{F}\bar{4}3\text{m}$ structure occur. It is difficult to predict what the effect on T_c is because the ϕ_{crit}^{net} parameter becomes very anisotropic; small four-center hydrogen bond networks form for with $\phi_{crit}^{*,net} \equiv 0.8$ but extended hydrogen networks form across the entire cell at $\phi_{crit}^{net} = 0.5$. Such anisotropic behavior in large unit cells was not considered in the data for T_c^{net} [42], so the predicted T_c^{net} of 145 K for the distorted structure at 1 GPa could have a larger error bar than 60 K. Other examples of the $\text{F}\bar{4}3\text{m}$ model structure similarly illustrate that doping $\text{R}_8\text{H}_{23}\text{N}$ increases T_c^{net} by 30-50 K. As the highest predicted T_c^{net} comes from cubic (Mg,N)-doped ScH_3 , we note Mg and Sc form cubic alloys [67] and in fact have been studied as hydrogen storage materials [68, 69]. Based on our results and previous studies [29, 33, 55], we find it likely that these doped $[\text{Sc},\text{Y}]_8\text{H}_{23-\delta}[\text{N},\text{O}]$ examples with extremely high predicted T_c are synthesizable and dynamically stable with compression.

We note again T_c^{net} only reproduces T_c from Eliashberg calculations within $\pm 60\text{ K}$, so some examples presented may in fact have T_c exceeding 270 K. It is likely that the T_c for the structures presented here is large in a narrow pressure range, based on Eliashberg calculations on YH_3 [70] and experiments on N-doped LuH_3 [37, 71]. We remark that preliminary constrained DFT calculations indicate strong correlation effects may be present in these systems for the same reasons as presented in Ref. [72]; that is, DFT struggles to represent the near-neutral hydrogen atoms present in $\text{RH}_{3-\delta}$ and how its charge fluctuations impacts the electronic structure. A more thorough investigation of these effects is underway.

In summary, we present model structures based on doped supercells of FCC RH_3 to adopt their dynamical

stability properties at low pressures while tuning their electronic properties. These supercells have been engineered to have high T_c s with upper estimates of $220 \pm 60\text{ K}$. We end by remarking that it is compelling that the highest predicted T_c using our methodology comes from (Mg,N)-doped ScH_3 , which features both Ashcroft's proposal for hydrogen-dominant metallic alloys [4] and Feynman's guess that the highest temperature superconductor would be Sc-based [73].

MATERIALS AND METHODS

We use density functional theory (DFT) [74–76] and DFT+U [77, 78] first-principles electronic structure calculations to study the examples built using our proposed model structures (Fig. 1). The SSSP database [79] was used to vet pseudopotentials for convergence of the computed pressure, phonon frequencies, and formation energies. Each relaxed structure had remaining forces under $1\text{e-}5\text{ Ry/Bohr}$, and energy differences were under $1\text{e-}5\text{ Ry}$. We used wavefunction plane-wave cutoffs of 75 Ry for the structures and charge density cutoffs of 300 Ry, though we performed convergence tests with higher values (especially for Sc-based compounds) and found no differences. We generally used tight k-meshes corresponding to 0.13 \AA^{-1} , but did convergence tests with more k-points as needed. We used *Quantum Espresso's* default atomic projections for the PDOS calculations. The *phonopy* software [60] was used to compute phonon dispersions and generate the eigenvectors for atomic displacements.

The Allen-Dynes formula for T_c takes the form

$$T_c \approx f_1 f_2 \frac{\omega_{ln}}{1.20} \exp\left\{-1.04\left(\frac{1+\lambda}{\lambda-\mu^*(1-0.62\lambda)}\right)\right\} \quad (1)$$

$$f_1 = \left[1 + \left(\frac{\lambda}{\Lambda_1}\right)^{3/2}\right]^{1/3} \quad f_2 = 1 + \frac{\lambda^2}{\lambda^2 + \Lambda_2^2} \left(\frac{\bar{\omega}_2}{\omega_{ln}} - 1\right) \quad (2)$$

$$\Lambda_1 = 2.46(1 + 3.8\mu^*) \quad \Lambda_2 = 1.82(1 + 6.3\mu^*) \frac{\bar{\omega}_2}{\omega_{ln}} \quad (3)$$

$$\omega_{ln} \equiv \exp\left(\frac{1}{\lambda} \int_0^\infty \frac{\alpha^2 f(\omega)}{\omega} \log(\omega) d\omega\right) \quad (4)$$

$$\bar{\omega}_2 \equiv \frac{\int_0^\infty \alpha^2 f(\omega) \omega d\omega}{\int_0^\infty \alpha^2 f(\omega) / \omega d\omega} \quad (5)$$

To study large amounts of stoichiometries in our model structures and try to maximize T_c , we take advantage of the established correlation between certain hydride electronic properties and the isotropic Eliashberg T_c [42], which yields a method to roughly estimate T_c . The T_c

estimator takes the form

$$T_c^{net} \approx 750\Phi - 85 \quad (\text{Kelvin}) \quad (6)$$

$$\Phi \equiv \phi_{iso}^{net} \times H_f \times \sqrt[3]{\text{DOS}_{H,rel}(E_F)} \quad (7)$$

$$H_f \equiv \frac{\# \text{ of H forming network}}{\# \text{ of atoms in unit cell}} \quad (8)$$

$$\text{DOS}_{H,rel}(E_F) \equiv \frac{\text{DOS}_H(E_F)}{\text{DOS}_{tot}(E_F)} \quad (9)$$

$$(10)$$

where ϕ_{iso}^{net} is the critical hydrogen networking isovalue [42] which roughly measures the bonding strength/connectivity of the hydrogen sublattice. It is determined by the isovalue in which the electron local-

ization function (ELF) of electrons centered on different hydrogen atoms begin to overlap. H_f is the fraction of hydrogen in the unit cell forming a network with overlapping ELF from different hydrogen, and $\text{DOS}_{H,rel}(E_F)$ is the relative contribution of hydrogen states to the density of states at E_F . T_c^{net} has been established to reproduce the computed isotropic Eliashberg T_c of hundreds of hydrides within ± 60 K [42], which we find acceptable to identify material candidates to look further into.

Acknowledgements. This research was supported by the U.S. National Science Foundation (NSF, DMR-2104881; R.H.), the U.S. Department of Energy-National Nuclear Security Administration (DOE-NNSA) through the Chicago/DOE Alliance Center (DE-NA0003975; A.D., R.H.), the DOE Office of Science (DE-SC0020340, R.H.), and NSF SI2-SSE (Grant 1740112; H.P.).

-
- [1] H. K. Onnes, The superconductivity of mercury, *Comm. Phys. Lab. Univ. Leiden* **122**, 124 (1911).
- [2] N. W. Ashcroft, Metallic hydrogen: A high-temperature superconductor?, *Phys. Rev. Lett.* **21**, 1748 (1968).
- [3] V. L. Ginzburg, The problem of high-temperature superconductivity, *Annual Review of Materials Science* **2**, 663 (1972).
- [4] N. W. Ashcroft, Hydrogen dominant metallic alloys: high temperature superconductors?, *Phys. Rev. Lett.* **92**, 187002 (2004).
- [5] M. Somayazulu, M. Ahart, A. K. Mishra, Z. M. Geballe, M. Baldini, Y. Meng, V. V. Struzhkin, and R. J. Hemley, Evidence for superconductivity above 260 K in lanthanum superhydride at megabar pressures, *Phys. Rev. Lett.* **122**, 027001 (2019).
- [6] A. Drozdov, P. Kong, V. Minkov, S. Besedin, M. Kuzovnikov, S. Mozaffari, L. Balicas, F. Balakirev, D. Graf, V. Prakapenka, *et al.*, Superconductivity at 250 K in lanthanum hydride under high pressures, *Nature* **569**, 528 (2019).
- [7] E. Snider, N. Dasenbrock-Gammon, R. McBride, X. Wang, N. Meyers, K. V. Lawler, E. Zurek, A. Salamat, and R. P. Dias, Synthesis of yttrium superhydride superconductor with a transition temperature up to 262 K by catalytic hydrogenation at high pressures, *Phys. Rev. Lett.* **126**, 117003 (2021).
- [8] P. Kong, V. S. Minkov, M. A. Kuzovnikov, A. P. Drozdov, S. P. Besedin, S. Mozaffari, L. Balicas, F. F. Balakirev, V. B. Prakapenka, S. Chariton, *et al.*, Superconductivity up to 243 K in the yttrium-hydrogen system under high pressure, *Nature Comm.* **12**, 5075 (2021).
- [9] I. A. Troyan, D. V. Semenok, A. G. Kvashnin, A. V. Sadakov, O. A. Sobolevskiy, V. M. Pudalov, A. G. Ivanova, V. B. Prakapenka, E. Greenberg, A. G. Gavriliuk, *et al.*, Anomalous high-temperature superconductivity in YH_6 , *Adv. Mater.* **33**, 2006832 (2021).
- [10] K. P. Hilleke and E. Zurek, Tuning chemical precompression: Theoretical design and crystal chemistry of novel hydrides in the quest for warm and light superconductivity at ambient pressures, *J. Appl. Phys.* **131**, 070901 (2022).
- [11] H. Liu, I. I. Naumov, R. Hoffmann, N. W. Ashcroft, and R. J. Hemley, Potential high- T_c superconducting lanthanum and yttrium hydrides at high pressure, *Proc. Nat. Acad. Sci.* **114**, 6990 (2017).
- [12] F. Peng, Y. Sun, C. J. Pickard, R. J. Needs, Q. Wu, and Y. Ma, Hydrogen clathrate structures in rare earth hydrides at high pressures: possible route to room-temperature superconductivity, *Phys. Rev. Lett.* **119**, 107001 (2017).
- [13] D. V. Semenok, I. A. Troyan, A. G. Ivanova, A. G. Kvashnin, I. A. Kruglov, M. Hanfland, A. V. Sadakov, O. A. Sobolevskiy, K. S. Pervakov, I. S. Lyubutin, *et al.*, Superconductivity at 253 K in lanthanum–yttrium ternary hydrides, *Materials Today* **48**, 18 (2021).
- [14] Y. Song, J. Bi, Y. Nakamoto, K. Shimizu, H. Liu, B. Zou, G. Liu, H. Wang, and Y. Ma, Stoichiometric ternary superhydride LaBeH_8 as a new template for high-temperature superconductivity at 110 K under 80 GPa, *Phys. Rev. Lett.* **130**, 266001 (2023).
- [15] S. Chen, Y. Qian, X. Huang, W. Chen, J. Guo, K. Zhang, J. Zhang, H. Yuan, and T. Cui, High-temperature superconductivity up to 223 K in the Al stabilized metastable hexagonal lanthanum superhydride, *National Science Review* **11**, nwad107 (2024).
- [16] X. Liang, A. Bergara, X. Wei, X. Song, L. Wang, R. Sun, H. Liu, R. J. Hemley, L. Wang, G. Gao, *et al.*, Prediction of high- T_c superconductivity in ternary lanthanum borohydrides, *Phys. Rev. B* **104**, 134501 (2021).
- [17] Y. Sun, S. Sun, X. Zhong, and H. Liu, Prediction for high superconducting ternary hydrides below megabar pressure, *J. Physics: Condensed Matter* **34**, 505404 (2022).
- [18] R. Koshiji, M. Fukuda, M. Kawamura, and T. Ozaki, Prediction of quaternary hydrides based on densest ternary sphere packings, *Phys. Rev. Mater.* **6**, 114802 (2022).
- [19] K. Dolui, L. J. Conway, C. Heil, T. A. Strobel, R. P. Prasankumar, and C. J. Pickard, Feasible route to high-temperature ambient-pressure hydride superconductivity, *Physical Review Letters* **132**, 166001 (2024).
- [20] G. M. Shutov, D. V. Semenok, I. A. Kruglov, and A. R. Oganov, Ternary superconducting hydrides in the La–Mg–H system, *Mater. Today Phys.* **40**, 101300 (2024).

- [21] F. Zheng, Z. Zhang, Z. Wu, S. Wu, Q. Lin, R. Wang, Y. Fang, C.-Z. Wang, V. Antropov, Y. Sun, *et al.*, Prediction of ambient pressure superconductivity in cubic ternary hydrides with MH₆ octahedra, *Mater. Today Phys.*, 101374 (2024).
- [22] X. Liang, X. Wei, E. Zurek, A. Bergara, P. Li, G. Gao, and Y. Tian, Design of high-temperature superconductors at moderate pressures by alloying AlH₃ or GaH₃, *Matter Radiat. at Extremes* **9** (2024).
- [23] A.-M. Racu and J. Schoenes, Strong correlations in YH_{3- δ} evidenced by raman spectroscopy, *Phys. Rev. Lett.* **96**, 017401 (2006).
- [24] M. Shao, S. Chen, W. Chen, K. Zhang, X. Huang, and T. Cui, Superconducting ScH₃ and LuH₃ at megabar pressures, *Inorg. Chem.* **60**, 15330 (2021).
- [25] T. Lu, S. Meng, and M. Liu, Electron-phonon interactions in LuH₂, LuH₃, and LuN, arXiv preprint arXiv:2304.06726 (2023).
- [26] P. P. Ferreira, L. J. Conway, A. Cucciari, S. Di Cataldo, F. Giannessi, E. Kogler, L. T. Eleno, C. J. Pickard, C. Heil, and L. Boeri, Search for ambient superconductivity in the Lu-N-H system, *Nature Comm.* **14** (2023).
- [27] D. Dangic, P. Garcia-Goiricelaya, Y.-W. Fang, J. Ibanez-Azpiroz, and I. Errea, Ab initio study of the structural, vibrational, and optical properties of potential parent structures of nitrogen-doped lutetium hydride, *Phys. Rev. B* **108**, 064517 (2023).
- [28] A. Meninno and I. Errea, Ab initio study of metastable occupation of tetrahedral sites in palladium hydrides and its impact on superconductivity, *Phys. Rev. B* **107**, 024504 (2023).
- [29] S. Van der Molen, D. Nagengast, A. Van Gogh, J. Kalkman, E. S. Kooij, J. Rector, and R. Griessen, Insulating fcc YH_{3- δ} stabilized by MgH₂, *Phys. Rev. B* **63**, 235116 (2001).
- [30] R. Kataoka, T. Kimura, N. Takeichi, and A. Kamegawa, Stabilization of face-centered cubic high-pressure phase of REH₃ (RE= Y, Gd, Dy) at ambient pressure by alkali or alkaline-earth substitution, *Inorganic Chemistry* **57**, 4686 (2018).
- [31] R. Kataoka, T. Kojima, K. Tada, M. Kitta, N. Takeichi, K. Sakaki, M. Nozaki, T. Kimura, and A. Kamegawa, Face-centered-cubic yttrium trihydride high-pressure phase stabilized at ambient pressures by mechanical milling, *Materialia* **15**, 100956 (2021).
- [32] R. Kataoka, N. Taguchi, M. Kitta, N. Takeichi, R. Utsumi, H. Saitoh, M. Nozaki, and A. Kamegawa, The origin of the highly crystallized face-centered cubic YH₃ high-pressure phase when quenched to ambient condition, *Mater. Today Comm.* **31**, 103265 (2022).
- [33] S. Villa-Cortés and O. De la Peña-Seaman, Superconductivity on ScH₃ and YH₃ hydrides: Effects of applied pressure in combination with electron-and hole-doping on the electron-phonon coupling properties, *Chinese J. Physics* **77**, 2333 (2022).
- [34] Z. Ouyang, M. Gao, and Z.-Y. Lu, Superconductivity at ambient pressure in hole-doped LuH₃, arXiv preprint arXiv:2306.13981 (2023).
- [35] X. Hao, X. Wei, H. Liu, X. Song, R. Sun, G. Gao, and Y. Tian, First-principles calculations on structural stability and electronic properties of nitrogen-doped lutetium hydrides under pressure, *Physical Review Research* **5**, 043238 (2023).
- [36] N. Dasenbrock-Gammon, E. Snider, R. McBride, H. Pasan, D. Durkee, N. Khalvashi-Sutter, S. Munasinghe, S. E. Dissanayake, K. V. Lawler, A. Salamat, *et al.*, Evidence of near-ambient superconductivity in a N-doped lutetium hydride, *Nature* **615**, 244 (2023).
- [37] N. P. Salke, A. C. Mark, M. Ahart, and R. J. Hemley, Evidence for near ambient superconductivity in the Lu-NH system, arXiv preprint arXiv:2306.06301 (2023).
- [38] X. Li, Y. Wang, Y. Fu, S. A. Redfern, S. Jiang, P. Zhu, and T. Cui, Stabilization of high-pressure phase of face-centered cubic lutetium trihydride at ambient conditions, *Advanced Science*, 2401642 (2024).
- [39] X. Liang, Z. Lin, J. Zhang, J. Zhao, S. Feng, W. Lu, G. Wang, L. Shi, N. Wang, P. Shan, *et al.*, Observation of flat band and van hove singularity in nitrogen doped lutetium hydride, arXiv preprint arXiv:2308.16420 (2023).
- [40] A. Denchfield, H. Park, and R. J. Hemley, Electronic structure of nitrogen-doped lutetium hydrides, *Phys. Rev. Mater.* **8**, L021801 (2024).
- [41] A. Denchfield, F. Belli, E. Zurek, H. Park, and R. J. Hemley, Quantum stabilization and flat hydrogen-based bands of nitrogen-doped lutetium hydride, arXiv preprint arXiv:2403.01350 (2024).
- [42] F. Belli, T. Novoa, J. Contreras-Garcia, and I. Errea, Strong correlation between electronic bonding network and critical temperature in hydrogen-based superconductors, *Nature Comm.* **12**, 5381 (2021).
- [43] H. Jeon, C. Wang, S. Liu, J. M. Bok, Y. Bang, and J.-H. Cho, Electron-phonon coupling and superconductivity in an alkaline earth hydride CaH₆ at high pressures, *New J. Physics* **24**, 083048 (2022).
- [44] Y.-W. Fang, D. Dangic, and I. Errea, Assessing the feasibility of near-ambient conditions superconductivity in the lu-nh system, *Communications Materials* **5**, 61 (2024).
- [45] S. Poncé, E. R. Margine, C. Verdi, and F. Giustino, Epw: Electron-phonon coupling, transport and superconducting properties using maximally localized wannier functions, *Computer Physics Comm.* **209**, 116 (2016).
- [46] P. Allen and R. Dynes, Superconductivity at very strong coupling, *J. Phys. C: Solid State Physics* **8**, L158 (1975).
- [47] E. R. Margine and F. Giustino, Anisotropic migdaliashberg theory using wannier functions, *Phys. Rev. B* **87**, 024505 (2013).
- [48] L. Ma, K. Wang, Y. Xie, X. Yang, Y. Wang, M. Zhou, H. Liu, X. Yu, Y. Zhao, H. Wang, *et al.*, High-temperature superconducting phase in clathrate calcium hydride CaH₆ up to 215 K at a pressure of 172 GPa, *Physical Review Letters* **128**, 167001 (2022).
- [49] H. Wang, J. S. Tse, K. Tanaka, T. Iitaka, and Y. Ma, Superconductive sodalite-like clathrate calcium hydride at high pressures, *Proceedings of the National Academy of Sciences* **109**, 6463 (2012).
- [50] Z. Shao, D. Duan, Y. Ma, H. Yu, H. Song, H. Xie, D. Li, F. Tian, B. Liu, and T. Cui, Unique phase diagram and superconductivity of calcium hydrides at high pressures, *Inorganic chemistry* **58**, 2558 (2019).
- [51] K. Yang, H. Sun, H. Chen, L. Chen, B. Li, and W. Lu, Stable structures and superconducting properties of Ca-H compounds under pressure, *J. Phys. Condens. Matter* **34**, 355401 (2022).
- [52] D. Papaconstantopoulos, M. Mehl, and E. Economou, High-temperature superconductivity in the Ca-Sc-H system, *Phys. Rev. B* **108**, 224508 (2023).

- [53] R. A. Klein, R. Balderas-Xicohténcatl, J. P. Maehlen, T. J. Udovic, C. M. Brown, R. Delaplane, Y. Cheng, R. V. Denys, A. J. Ramirez-Cuesta, and V. A. Yartys, Neutron vibrational spectroscopic evidence for short H-H contacts in the $R\text{NiInH}_{1.4;1.6}$ ($R = \text{Ce, La}$) metal hydride, *J. Alloys and Compounds* **894**, 162381 (2022).
- [54] J. Liu, X.-B. Li, H. Zhang, W.-J. Yin, H.-B. Zhang, P. Peng, and L.-M. Liu, Electronic structures and optical properties of two-dimensional ScN and YN nanosheets, *J. Appl. Phys.* **115** (2014).
- [55] R. Kataoka, T. Kimura, K. Sakaki, M. Nozaki, T. Kojima, K. Ikeda, T. Otomo, N. Takeichi, and A. Kamegawa, Facile synthesis of LiH-stabilized face-centered-cubic YH₃ high-pressure phase by ball milling process, *Inorganic chemistry* **58**, 13102 (2019).
- [56] R. Kataoka, M. Nozaki, T. Kimura, K. Sakaki, T. Kojima, K. Ikeda, T. Otomo, N. Takeichi, and A. Kamegawa, Zirconium hydride-stabilized yttrium hydride (ZSY): Stabilization of a face-centered cubic YH₃ phase by Zr substitution, *J. Alloys and Compounds* **851**, 156071 (2021).
- [57] A.-M. Carsteanu, M. Rode, D. Zur, J. Schoenes, A. Borgschulte, and R. Westerwaal, Distortion of the fcc lattice in superstoichiometric $\beta\text{-YH}_{2+\delta}$ and cubic $\text{YH}_{3-\eta}$ thin films, *J. Alloys Compd.* **404-406**, 82 (2005).
- [58] Y. Sun, Y. Wang, X. Zhong, Y. Xie, and H. Liu, High-temperature superconducting ternary Li-R-H superhydrides at high pressures ($R = \text{Sc, Y, La}$), *Phys. Rev. B* **106**, 024519 (2022).
- [59] X. Liang, A. Bergara, L. Wang, B. Wen, Z. Zhao, X.-F. Zhou, J. He, G. Gao, and Y. Tian, Potential high- T_c superconductivity in CaYH_{12} under pressure, *Phys. Rev. B* **99**, 100505 (2019).
- [60] A. Togo, First-principles phonon calculations with phonopy and phono3py, *J. Physical Society of Japan* **92**, 012001 (2023).
- [61] H. Liu, I. I. Naumov, Z. M. Geballe, M. Somayazulu, J. S. Tse, and R. J. Hemley, Dynamics and superconductivity in compressed lanthanum superhydride, *Physical Review B* **98**, 100102 (2018).
- [62] I. Errea, F. Belli, L. Monacelli, A. Sanna, T. Koretsune, T. Tadano, R. Bianco, M. Calandra, R. Arita, F. Mauri, *et al.*, Quantum crystal structure in the 250-kelvin superconducting lanthanum hydride, *Nature* **578**, 66 (2020).
- [63] Y. Quan, S. S. Ghosh, and W. E. Pickett, Compressed hydrides as metallic hydrogen superconductors, *Phys. Rev. B* **100**, 184505 (2019).
- [64] N. Zapp, H. Auer, and H. Kohlmann, YHO, an air-stable ionic hydride, *Inorganic Chemistry* **58**, 14635 (2019).
- [65] A. Jain, J. Montoya, S. Dwaraknath, N. E. Zimmermann, J. Dagdelen, M. Horton, P. Huck, D. Winston, S. Cholia, S. P. Ong, *et al.*, The materials project: Accelerating materials design through theory-driven data and tools, *Handbook of Materials Modeling: Methods: Theory and Modeling*, 1751 (2020).
- [66] T. Kume, H. Ohura, T. Takeichi, A. Ohmura, A. Machida, T. Watanuki, K. Aoki, S. Sasaki, H. Shimizu, and K. Takemura, High-pressure study of ScH₃: Raman, infrared, and visible absorption spectroscopy, *Phys. Rev. B* **84**, 064132 (2011).
- [67] O. t. Schob and E. Parthé, AB compounds with Sc, Y and rare earth metals. I. Scandium and yttrium compounds with CrB and CsCl structure, *Acta Crystallographica* **19**, 214 (1965).
- [68] W. Kalisvaart, R. Niessen, and P. Notten, Electrochemical hydrogen storage in mgsc alloys: A comparative study between thin films and bulk materials, *J. Alloys Compd.* **417**, 280 (2006).
- [69] S. Al, N. Cavdar, and N. Arıkan, Computational evaluation of comprehensive properties of mgx3h8 ($x = \text{sc, ti}$ and zr) as effective solid state hydrogen storage materials, *J. Energy Storage* **80**, 110402 (2024).
- [70] D. Y. Kim, R. H. Scheicher, and R. Ahuja, Predicted high-temperature superconducting state in the hydrogen-dense transition-metal hydride YH₃ at 40 K and 17.7 GPa, *Physical review letters* **103**, 077002 (2009).
- [71] R. Dias, N. Dasenbrock-Gammon, E. Snider, R. McBride, H. Pasan, D. Durkee, N. Khalvashi-Sutter, S. Disanayake, K. Lawler, and A. Salamat, Observation of room temperature superconductivity in hydride at near ambient pressure, *Bulletin of the American Physical Society* (2023).
- [72] R. Eder, H. Pen, and G. Sawatzky, Kondo-lattice-like effects of hydrogen in transition metals, *Physical Review B* **56**, 10115 (1997).
- [73] D. Goodstein and J. Goodstein, Richard feynman and the history of superconductivity, *Physics in Perspective* **2**, 30 (2000).
- [74] W. Kohn and L. J. Sham, Self-consistent equations including exchange and correlation effects, *Physical Review* **140**, A1133 (1965).
- [75] P. Giannozzi, S. Baroni, N. Bonini, M. Calandra, R. Car, C. Cavazzoni, D. Ceresoli, G. L. Chiarotti, M. Cococcioni, I. Dabo, *et al.*, Quantum espresso: a modular and open-source software project for quantum simulations of materials, *J. Physics: Cond. Matter* **21**, 395502 (2009).
- [76] P. Giannozzi, O. Andreussi, T. Brumme, O. Bunau, M. B. Nardelli, M. Calandra, R. Car, C. Cavazzoni, D. Ceresoli, M. Cococcioni, *et al.*, Advanced capabilities for materials modelling with quantum espresso, *J. Physics: Cond. Matter* **29**, 465901 (2017).
- [77] Y.-C. Wang, Z.-H. Chen, and H. Jiang, The local projection in the density functional theory plus U approach: A critical assessment, *J. Chem. Phys.* **144**, 144106 (2016).
- [78] S. A. Tolba, K. M. Gameel, B. A. Ali, H. A. Almossalami, and N. K. Allam, The DFT+U: Approaches, accuracy, and applications, *Density Functional Calculations-Recent Progresses of Theory and Application*, edited by G. Yang, Chapter 1 **1**, 5772 (2018).
- [79] G. Prandini, A. Marrazzo, I. E. Castelli, N. Mounet, and N. Marzari, Precision and efficiency in solid-state pseudopotential calculations, *npj Comp. Mater.* **4**, 1 (2018).